Abstracta

Ano XVII - N. 05

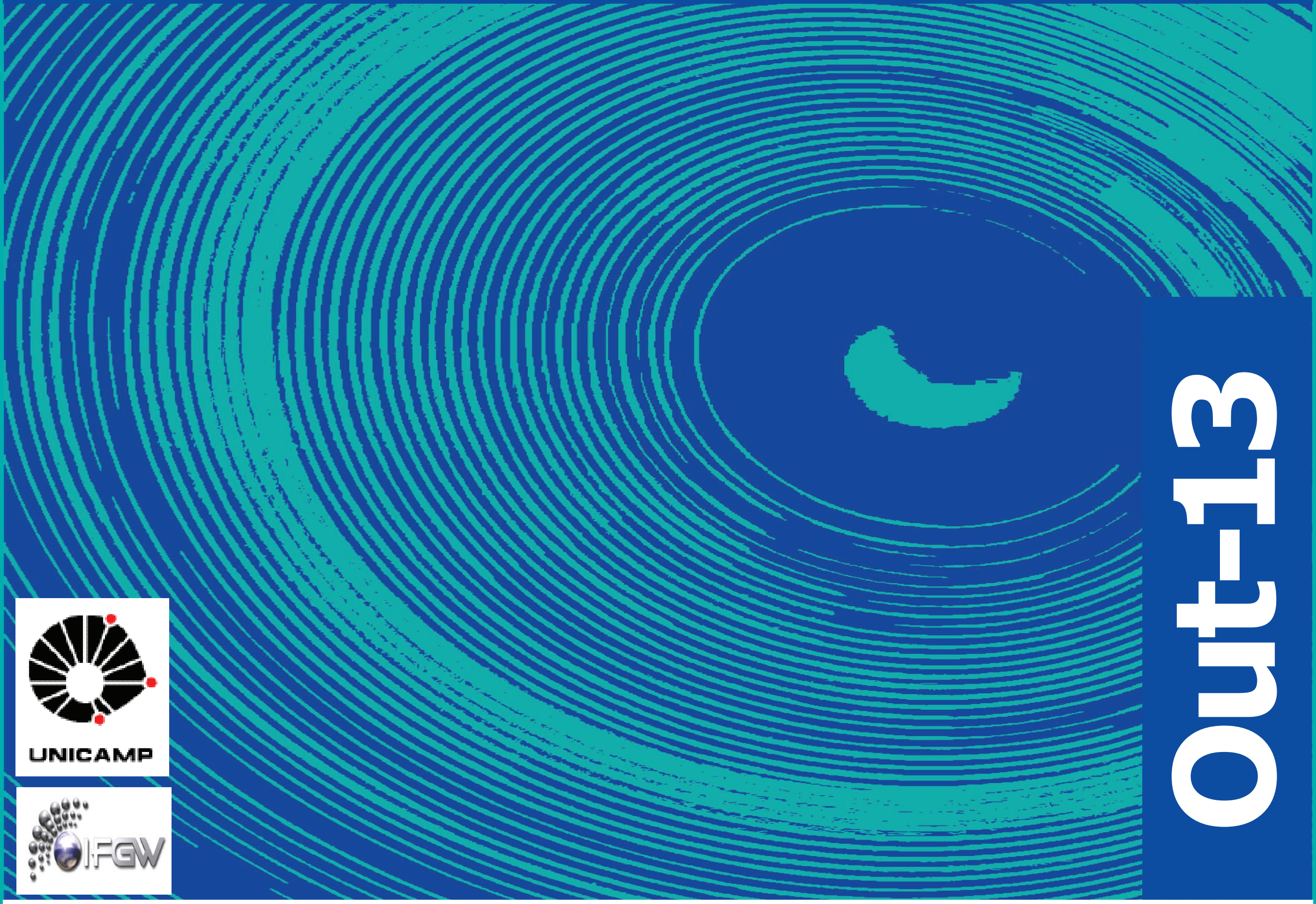

Trabalhos Publicados
P246-13 à P289-13

Proocedings
P290-13

Defesas de Dissertações do IFGW
D018-13 à D020-13

Defesas de Teses do IFGW
T011-13 à T015-13

Trabalhos Publicados

[P246-2013] "An updated analysis on the rise of the hadronic total cross-section at the lhc energy region"

Menon, M. J.*; Silva, P. V. R. G.*

A forward amplitude analysis on pp and (p) over barp elastic scattering above 5 GeV is presented. The dataset includes the recent high-precision TOTEM measurements of the pp total and elastic (integrated) cross-sections at 7 TeV and 8 TeV. Following previous works, the leading high-energy contribution for the total cross-section (sigma(tot)) is parametrized as ln(gamma) (s/s(h)), where gamma and s(h) are free real fit parameters. Singly-subtracted derivative dispersion relations are used to connect sigma(tot) and the rho parameter (rho) in an analytical way. Different fit procedures are considered, including individual fits to sigma(tot) data, global fits to sigma(tot) and rho data, constrained and unconstrained data reductions. The results favor a rise of the sigma(tot) faster than the log-squared bound by Froissart and Martin at the LHC energy region. The parametrization for sigma(tot) is extended to fit the elastic cross-section (sigma(el)) data with satisfactory results. The analysis indicates an asymptotic ratio sigma(el)/sigma(tot) consistent with 1/3 (as already obtained in a previous work). A critical discussion on the correlation, practical role and physical implications of the parameters gamma and s(h) is presented. The discussion confronts the 2002 prediction of sigma(tot) by the COMPETE Collaboration and the recent result by the Particle Data Group (2012 edition of the Review of Particle Physics). Some conjectures on possible implications of a fast rise of the proton-proton total cross-section at the highest energies are also presented.

International Journal Of Modern Physics A 28[20], UNSP 1350099, 2013. DOI: 10.1142/S0217751X13500991

[P247-2013] "Bending of Layer-by-Layer Films Driven by an External Magnetic Field"

Miyazaki, C. M.; **Riul, A.***; Dos Santos, D. S.; Ferreira, M.; Constantino, C. J. L.; Pereira-da-Silva, M. A.; Paupitz, R.; **Galvao, D. S.***; Oliveira, O. N.

We report on optimized architectures containing layer-by-layer (LbL) films of natural rubber latex (NRL), carboxymethyl-chitosan (CMC) and magnetite (Fe3O4) nanoparticles (MNPs) deposited on flexible substrates, which could be easily bent by an external magnetic field. The mechanical response depended on the number of deposited layers and was explained semi-quantitatively with a fully atomistic model, where the LbL film was represented as superposing layers of hexagonal graphene-like atomic arrangements deposited on a stiffer substrate. The bending with no direct current or voltage being applied to a supramolecular structure containing biocompatible and antimicrobial materials represents a proof-of-principle experiment that is promising for tissue engineering applications in biomedicine.

International Journal Of Molecular Sciences 14[7], 12953-12969 DOI: 10.3390/ijms140712953

[P248-2013] "Between-individual variation drives the seasonal dynamics in the trophic niche of a Neotropical marsupial"

Pires, M. M.; Martins, E. G.; **Araujo, M. S.***; dos Reis, S. F.

The dynamics of population niches result from the variation in resource use within individuals and also from the variation between individuals. The prevalence of one mechanism or the other leads to competing hypotheses about the major mechanisms underlying the empirical observations of the contraction/expansion dynamics of the trophic niche in natural populations. In this study, we investigated how within- and between-individual variation in resource use shapes the food niche dynamics of the woolly mouse opossum, Marmosa paraguayana (Didelphimorphia: Didelphidae), in a remnant of the highly seasonal Cerrado in south-eastern Brazil. To do so, we analysed the faecal samples of live-trapped individuals to determine their diets within the wet and dry seasons. In addition to a seasonal shift in the composition of the diet, the population trophic niche was significantly wider during the dry season than the wet season. This expansion resulted from larger between--individual variation in the dry season that was not related to sex preferences, whereas the individual niche widths did not significantly increase from the wet to the dry seasons. Our findings add to the growing list of animal populations that show individual-level variation in resource use. Furthermore, these results represent a pattern of individual-level response to seasonal changes that is different from patterns reported for other organisms. We suggest that a pathway to build more realistic foraging models and produce more accurate predictions on population and community dynamics is to consider between-individual variation and short-term niche dynamics.

Austral Ecology 38[6], 664-671, 2013. DOI: 10.1111/aec.12011

[P249-2013] "Conditions for neutral speciation via isolation by distance"

Baptestini, E. M.*; de Aguiar, M. A. M.*; Bar-Yam, Y.

The branching of new species from an ancestral population requires the evolution of reproductive isolation between groups of individuals. Geographic separation of sub-populations by natural barriers, if sustained for sufficiently long times, may lead to the accumulation of independent genetic changes in each group and to mating incompatibilities (Mayr, 2001; Fitzpatrick et al., 2009). A similar phenomenon may occur in the absence of barriers via isolation by distance if the population is distributed over large areas (de Aguiar et al., 2009; Etienne and Haegeman, 2011; Gavrilets et al., 2000). The first demonstration of this process was based on computer simulations employing agent-based models. Recently, analytical results were derived combining network theory, to model the spatial structure of the population, and an ansatz that accounts for the effect of forbidding mating between individuals that are too different genetically (de Aguiar and Bar-Yam, 2011). The main result obtained with this approach is an expression that indicates when speciation is possible as a function of the parameters describing the population. The aim of this work is to test this analytical result by comparing it with numerical simulations for a hermaphroditic population (de Aguiar et al., 2009) and for a population whose individuals are explicitly separated into males and females (Baptestini et al., 2013). We show that the analytical formula is indeed a very good overall description of the simulations and that the exponents describing dependence of the critical threshold of speciation with the parameters are in good agreement with the simulations.

Journal Of Theoretical Biology 335, 51-56, 2013. DOI: 10.1016/j.jtbi.2013.06.011

[P250-2013] "Cross sections for electron collisions with dimethyl ether"

Sugohara, R. T.; Homem, M. G. P.; Iga, I.; de Souza, G. L. C.; Machado, L. E.; Ferraz, J. R.; dos Santos, A. S.; **Brescansin, L. M.***; Lucchese, R. R.; Lee, M. T.

We report a joint theoretical-experimental investigation of electron collision with dimethyl ether (DME) in the low- and intermediate-energy ranges. Experimental absolute differential, integral, and momentum-transfer cross sections for elastic e(-)--DME scattering are reported in the 100-1000 eV energy range.

Our measurements were performed using a crossed electron-beam-molecular-beam geometry. The angular distribution of the scattered electrons was converted to absolute cross section using the relative flow technique. Theoretically, elastic differential, integral, and momentum-transfer cross sections, as well as the grand-total and total absorption cross sections for electron collision with DME are calculated in the 1-1000 eV energy range. A single-center-expansion technique combined with the Pade approximant method is used in our calculations. A comparison between the present experimental and theoretical data shows very good agreement. Moreover, comparison with theoretical and experimental data for e(-)-ethanol (an isomer of DME) scattering shows interesting isomeric effects.

Physical Review A 88[2], 022709, 2013. DOI: 10.1103/PhysRevA.88.022709

[P251-2013] "D Meson Elliptic Flow in Noncentral Pb-Pb Collisions at root(S)(NN)=2.76 TeV"

Abelev, B.; Adam, J.; Adamova, D.; Adare, A. M.; **Dash, A.*; Takahashi, J.***; et al.
ALICE Collaboration

Azimuthally anisotropic distributions of D-0, D+, and D*+ mesons were studied in the central rapidity region (vertical bar y vertical bar < 0.8) in Pb-Pb collisions at a center-of-mass energy root(S)(NN) = 2.76 TeV per nucleon-nucleon collision, with the ALICE detector at the LHC. The second Fourier coefficient upsilon(2) (commonly denoted elliptic flow) was measured in the centrality class 30%-50% as a function of the D meson transverse momentum p(T), in the range 2-16 GeV/c. The measured upsilon(2) of D mesons is comparable in magnitude to that of light-flavor hadrons. It is positive in the range 2 < p(T) < 6 GeV/c with 5.7 sigma significance, based on the combination of statistical and systematic uncertainties.

Physical Review Letters 111[10], 102301, 2013. DOI: 10.1103/PhysRevLett.111.102301

[P252-2013] "Emission of monochromatic microwave radiation from a nonequilibrium condensation of excited magnons"

Vannucchi, F. S.*; Vasconcellos, A. R.*; Luzzi, R.*

The observation of monochromatic emission of radiation from a nonequilibrium Bose-Einstein-like condensate of magnons suggests the possibility of creating a monochromatic microwave generator pumped by incoherent broadband sources. The device would have a tunable emitted frequency as a function of the applied constant magnetic field. We present an analysis of the mechanisms of interaction between the condensate of magnons and the radiation field producing the super-radiant emission of photons. The conditions for the emergence of the super-radiance are described, as well as an analysis of its dependence on the thickness of the sample and the applied static magnetic field intensity.

Applied Physics Letters 103[7], 072401, 2013. DOI: 10.1063/1.4818312

[P253-2013] "EPR Study of MnO and MnO2 Doped Barium Aluminoborate Glasses"

Giehl, J. M.*; Miranda, A. R.*; Pontuschka, W. M.; Navarro, M.; Da Costa, Z. M.

An off-equilibrium redox condition study of Mn2+ and Mn4+ ions added to the batch is reported for the case of the preparation of the barium aluminoborate glasses, by considering that the out of equilibrium reactions started already on the melt. It is shown that for lower dopant concentrations the relative concentrations of the oxidation states of the manganese are found out of equilibrium up to the added amount of 0.3 mol% of MnO2, but on doping with MnO, the equilibrium state is achieved at the MnO added amount of 0.07 mol%. The change of the redox condition of the manganese ions toward the equilibrium was studied by tracking the Mn2+ amount as a function of the doping concentration in the two cases of MnO and MnO2.

Journal Of Superconductivity And Novel Magnetism 26[6], 2295-2298, 2013. DOI: 10.1007/s10948-012-1457-9

[P254-2013] "Further investigation of the initial fission-track length and geometry factor in apatite fission-track thermochronology"

Soares, C. J.*; Guedes, S.*; Tello, C. A.; **Lixandrao, A. L.***; Osorio, A. M.; **Alencar, I*.**; Dias, A. N. C.; **Hadler, J.***

The external detector method (EDM) is a widely used technique in fission track thermochronology (FTT) in which two different minerals are concomitantly employed: spontaneous tracks are observed in apatite and induced ones in the muscovite external detector. They show intrinsic differences in detection and etching properties that should be taken into account. In this work, new geometry factor values, g, in apatite, were obtained by directly measuring the rho(ed)/rho(is) ratios and independently determined [GQR](ed/is) values through the measurement of projected lengths. Five mounts, two of which were large area prismatic sections and three samples composed of random-orientation pieces have been used to determine the g-values. A side effect of applying EDM is that the value of the initial confined induced fission track, L-0, is not measured in routine analyses. The L-0-value is an important parameter to quantify with good confidence the degree of annealing of the spontaneous fission tracks in unknown-age samples, and is essential for accurate thermal history modeling. The impact of using arbitrary L-0-values on the inference of sample thermal history is investigated and discussed. The measurement of the L-0-value for each sample to be dated using an extra irradiated apatite mount is proposed. This extra mount can be also used for determining the g value as an extension of the rho(ed)/rho(is) ratio method. Eight apatite samples from crystalline basement, with grains at random orientation, were used to determine the g-values. The results found are statistically in agreement with the values found for apatite samples (from Durango, Mexico) measured in prismatic section and also measured at random orientation. There was no observable variation in efficiency regarding crystal orientation, showing that it is relatively safe using non-prismatic grains, especially in samples with paucity of grains, as it is the case of most basin samples. Implications for the zeta-calibration and for the calibration of the direct (spectrometer-based) fission-track dating are also discussed.

American Mineralogist 98[8-9], 1381-1392, 2013. DOI: 10.2138/am.2013.4140

[P255-2013] "Improvement on direct ethanol fuel cell performance by using doped-Nafion (R) 117 membranes with Pt and Pt-Ru nanoparticles"

Battirola, L. C.; Schneider, J. F.; **Torriani, I. C. L.***; Tremiliosi, G.; Rodrigues, U. P.

Nafion (R) 117 membranes doped with Pt (4 x 10(-4) mol L-1 or 8 x 10(-4) mol L-1 H2PtCl6 solution), and with Pt-Ru (4 x 10(-4) mol L-1 H2PtCl6 and 2 x 10(-4) mol L-1 RuCl3 solutions) nanoparticles have been synthesized using a simple and scalable absorption-reduction method. The chemical integrity of the membranes was confirmed by C-13 and F-19 solid-state NMR. The pore microstructure of the membranes was preserved after the doping process, according to SAXS measurements.

The tests of the direct ethanol fuel cells (DEFC) performance at 90 degrees C exhibited up to 38% and 56% increase at the maximum power densities for Pt doped-Nafion (R) membrane from lower and higher concentration of H2PtCl6 solution, respectively, compared to bare Nafion membranes. Additionally, a Pt-Ru doped-membrane tested at 110 degrees C exhibited the highest power density. Such superior performances may be attributed to a synergistic effect between the extra amount of active catalytic sites inside the pore structure for the electrochemical oxidation of ethanol, thus preventing ethanol crossover, and the excellent proton migration properties conferred by the pore microstructure of Nafion (R). These results demonstrate that the doped-Nafion (R) membrane has a good capacity to improve the performance of DEFC, and provided further clarification on the synthesis process of polymer electrolyte doped-membranes in fuel cell technology.

International Journal Of Hydrogen Energy 38[27], 12060-12068, 2013. DOI: 10.1016/j.ijhydene.2013.06.126

[P256-2013] "Intermolecular interactions between imidazole derivatives intercalated in layered solids. Substituent group effect"

Gonzalez, M.; Lemus-Santana, A. A.; Rodriguez-Hernandez, J.; Aguirre-Velez, C. I.; **Knobel, M.***; Reguera, E.

This study sheds light on the intermolecular interactions between imidazole derive molecules (2-methyl-imidazole, 2-ethyl-imidazole and benzimidazole) intercalated in T[Ni(CN)(4)] layers to form a solid of formula unit T(ImD)(2)[Ni(CN)(4)]. These hybrid inorganic-organic solids were prepared by soft chemical routes and their crystal structures solved and refined from X-ray powder diffraction data. The involved imidazole derivative molecules were found coordinated through the pyridinic N atom to the axial positions for the metal T in the T[Ni(CN)(4)] layer. In the interlayers region ligand molecules from neighboring layers remain stacked in a face-to-face configuration through dipole-dipole and quadrupole-quadrupole interactions. These intermolecular interactions show a pronounced dependence on the substituent group and are responsible for an ImD--pillaring concatenation of adjacent layers. This is supported by the structural information and the recorded magnetic data in the 2-300 K temperature range. The samples containing Co and Ni are characterized by presence of spin-orbit coupling and pronounced temperature dependence for the effective magnetic moment except for 2-ethyl-imidazole related to the local distortion for the metal coordination environment. For this last one ligand a weak ferromagnetic ordering ascribed to a super-exchange interaction between T metals from neighboring layers through the ligands pi-pi interaction was detected.

Journal Of Solid State Chemistry 204, 128-135, 2013. DOI: 10.1016/j.jssc.2013.05.029

[P257-2013] "Low-energy positron scattering from iodomethane"

Varella, M. T. D.; Sanchez, S. D.; Bettega, M. H. F.; **Lima, M. A. P.***; Chiari, L.; Zecca, A.; Trainotti, E.; Brunger, M. J.

We report experimental total cross sections (TCSs) and calculated elastic integral cross sections (ICSs) for positron collisions with iodomethane (methyl iodide, CH3I). The experimental TCSs were obtained with a linear transmission technique, for energies from 0.1 up to 50 eV. The present TCS data agree well with those previously reported (Kimura et al 2001 J. Chem. Phys. 115 7442) at higher energies (above 7 eV), but significant discrepancies are found at the lower energies. The present ICS computations were performed with the Schwinger multichannel method (SMC) and the Born dipole approximation in the incident energy range from 0.1 eV up to 10 eV. Iodomethane poses a great challenge to theoretical descriptions of the collisions dynamics. In addition to the neglect of inelastic channels, the main difficulty found in the SMC approach is related to numerical limitations that prevent a thorough description of correlation-polarization effects. Although our ICS calculations do not compare well with the present TCS data, the results are encouraging, as iodomethane would challenge all the presently available computational approaches.

Journal Of Physics B-Atomic Molecular And Optical Physics 46[17], 175202, 2013. DOI: 10.1088/0953-4075/46/17/175202

[P258-2013] "Macroscopic quantum tunneling of magnetization explored by quantum-first-order reversal curves"

Beron, F.*; Novak, M. A.; Vaz, M. G. F.; Guedes, G. P.; **Knobel, M.*; Caldeira, A.*; Pirota, K. R. ***

A method to study the fundamental problem of quantum double well potential systems that display magnetic hysteresis is proposed. The method, coined quantum-first-order reversal curve (QFORC), is inspired by the first-order reversal curve, based on the Preisach model for hysteresis. We successfully tested the QFORC method in the hysteresis of the Mn12Ac molecular magnet, which is governed by macroscopic quantum tunneling of magnetization. The QFORC reproduces well the experimental magnetization behavior. It is possible to separate the thermal activation and tunneling contributions from the magnetization variation, as well as associate the magnetization jumps with specific quantum transitions.

Applied Physics Letters 103[5], 052407, 2013, DOI: 10.1063/1.4816131

[P259-2013] "Measurement of J/psi Azimuthal Anisotropy in Au plus Au Collisions at root s(NN)=200 GeV"

Adamczyk, L.; Adkins, J. K.; Agakishiev, G.; Aggarwal, M. M.; **Derradi de Souza, R.*; Takahashi, J.*; Vasconcelos, G. M. S.*; et al.**
STAR Collaboration

The measurement of J/psi azimuthal anisotropy is presented as a function of transverse momentum for different centralities in Au + Au collisions at root s(NN) = 200 GeV. The measured J/psi elliptic flow is consistent with zero within errors for transverse momentum between 2 and 10 GeV/c. Our measurement suggests that J/psi particles with relatively large transverse momenta are not dominantly produced by coalescence from thermalized charm quarks, when comparing to model calculations.

Physical Review Letters 111[5], 052301, 2013. DOI: 10.1103/PhysRevLett.111.052301

[P260-2013] "Measurement of masses in the t(t)over-tilde system by kinematic endpoints in pp collisions at root s=7 TeV"

Chatrchyan, S.; Khachatryan, V.; Sirunyan, A. M.; Tumasyan, A.; **Chinellato, J.*; Manganote, E. J. Tonelli*;** et al.
CMS Collaboration

A simultaneous measurement of the top-quark, W-boson, and neutrino masses is reported for t (t) over bar events selected in the dilepton final state from a data sample corresponding to an integrated luminosity of 5.0 fb(-1) collected by the CMS experiment in pp collisions at root s = 7 TeV. The analysis is based on endpoint determinations in kinematic distributions. When the neutrino and W-boson masses are constrained to their world-average values, a top-quark mass value of M-t = 173.9 +/- 0.9 (stat.)=(+ 1.7) (-2.1) (syst.) GeV is obtained. When such constraints are not used, the three particle masses are obtained in a simultaneous fit. In this unconstrained mode the study serves as a test of mass determination methods that may be used in beyond standard model physics scenarios where several masses in a decay chain may be unknown and undetected particles lead to underconstrained kinematics.

European Physical Journal C 73[7], 2494, 2013. DOI: 10.1140/epjc/s10052-013-2494-7

[P261-2013] "Measurement of neutral strange particle production in the underlying event in proton-proton collisions at root s=7 TeV"

Chatrchyan, S.; Khachatryan, V.; Sirunyan, A. M.; Tumasyan, A.; Adam, W.; **Chinellato, J.*; Tonelli Manganote, E. J.*;** et al.
CMS Collaboration

Measurements are presented of the production of primary K-S(0) and Lambda particles in proton-proton collisions at root s = 7 TeV in the region transverse to the leading charged-particle jet in each event. The average multiplicity and average scalar transverse momentum sum of K-S(0) and Lambda particles measured at pseudorapidities vertical bar eta vertical bar < 2 rise with increasing charged-particle jet p(T) in the range 1-10 GeV/c and saturate in the region 10-50 GeV/c. The rise and saturation of the strange-particle yields and transverse momentum sums in the underlying event are similar to those observed for inclusive charged particles, which confirms the impact-parameter picture of multiple parton interactions. The results are compared to recent tunes of the PYTHIA Monte Carlo event generator. The PYTHIA simulations underestimate the data by 15%-30% for K-S(0) mesons and by about 50% for Lambda baryons, a deficit similar to that observed for the inclusive strange-particle production in non-single-diffractive proton-proton collisions. The constant strange-to charged-particle activity ratios with respect to the leading jet p(T) and similar trends for mesons and baryons indicate that the multiparton-interaction dynamics is decoupled from parton hadronization, which occurs at a later stage.

Physical Review D 88[5], 2013. DOI: 10.1103/PhysRevD.88.052001

[P262-2013] "Measurement of the B-s(0) ->mu(+)mu(-) Branching Fraction and Search for B-0 -> mu(+)mu(-) with the CMS Experiment"

Chatrchyan, S.; Collaboration, C. M. S.; Khachatryan, V.; Sirunyan, A. M.; **Chinellato, J.*; Tonelli Manganote, E. J.*;** et al.

Results are presented from a search for the rare decays B-s(0) -> mu(+) mu(-) and B-0 -> mu(+) mu(-) in pp collisions at root s = 7 and 8 TeV, with data samples corresponding to integrated luminosities of 5 and 20 fb(-1), respectively, collected by the CMS experiment at the LHC. An unbinned maximum-likelihood fit to the dimuon invariant mass distribution gives a branching fraction 'B(B-s(0) -> mu(+)mu(-)) = (3.0(-0.9)(+1.0)) x 10(-9), where the uncertainty includes both statistical and systematic contributions. An excess of B-s(0) -> mu(+)mu(-) events with respect to background is observed with a significance of 4.3 standard deviations. For the decay B-0 -> mu(+) mu(-) an upper limit of 'B(B-0 -> mu(+) mu(-)) < 1.1 x 10(-9) at the 95% confidence level is determined. Both results are in agreement with the expectations from the standard model.

Physical Review Letters 111[10], 101804, 2013. DOI: 10.1103/PhysRevLett.111.101804

[P263-2013] "Measurement of the Lambda(0)(b) lifetime in pp collisions at root s=7 TeV"

Chatrchyan, S.; Khachatryan, V.; Sirunyan, A. M.; Tumasyan, A.; Adam, W.; **Chinellato, J.*; Tonelli Manganote, E. J.*;** et al.
CMS Collaboration

A measurement of the Lambda(0)(b) lifetime using the decay Lambda(0)(b) -> J/psi Lambda in protonproton collisions at root s = 7TeV is presented. The data set, corresponding to an integrated luminosity of about 5 fb(-1), was recorded with the CMS experiment at the Large Hadron Collider using triggers that selected dimuon events in the J/psi mass region. The Lambda(0)(b) lifetime is measured to be 1.503 +/- 0.052 (stat.) +/- 0.031 (syst.) ps

Journal Of High Energy Physics 7, 163, 2013. DOI: 10.1007/JHEP07(2013)163

[P264-2013] "Mid-rapidity anti-baryon to baryon ratios in pp collisions at root s=0.9, 2.76 and 7 TeV measured by ALICE"

Abbas, E.; Abelev, B.; Adam, J.; Adamova, D.; Adare, A. M.; **Dash, A.*; Takahashi, J.*;** et al.
ALICE Collaboration

The ratios of yields of anti-baryons to baryons probes the mechanisms of baryon-number transport. Results for (p) over bar /p, (Lambda) over bar/Lambda, (Xi) over bar (+)/(Xi) over bar (-) and (Omega) over bar (+)/(Omega) over bar (-) in pp collisions at root s = 0.9, 2.76 and 7 TeV, measured with the ALICE detector at the LHC, are reported. Within the experimental uncertainties and ranges covered by our measurement, these ratios are independent of rapidity, transverse momentum and multiplicity for all measured energies. The results are compared to expectations from event generators, such as PYTHIA and HIJING/B, that are used to model the particle production in pp collisions. The energy dependence of (p) over bar /p, (Lambda) over bar/(Lambda) over bar, (Xi) over bar (+)/(Xi) over bar (-) and (Omega) over bar (+)/(Omega) over bar (-), reaching values compatible with unity for root s = 7 TeV, complement the earlier (p) over bar /p measurement of ALICE. These dependencies can be described by exchanges with the Regge-trajectory intercept of alpha(J) approximate to 0.5, which are suppressed with increasing rapidity interval Delta y. Any significant contribution of an exchange not suppressed at large Delta y (reached at LHC energies) is disfavoured.

European Physical Journal C 73[7], 2496, 2013. DOI: 10.1140/epjc/s10052-013-2496-5

[P265-2013] "Modeling the ATP Production in Mitochondria"

Saa, A.; **Siqueira, K. M.***

We revisit here the mathematical model for ATP production in mitochondria introduced recently by Bertram, Pedersen, Luciani, and Sherman (BPLS) as a simplification of the more complete but intricate Magnus and Keizer's model. We identify some inaccuracies in the BPLS original approximations for two flux rates, namely the adenine nucleotide translocator rate J (ANT) and the calcium uniporter rate J (uni). We introduce new approximations for such flux rates and then analyze some of the dynamical properties of the model. We infer, from exhaustive numerical explorations, that the enhanced BPLS equations have a unique attractor fixed point for physiologically acceptable ranges of mitochondrial variables and respiration inputs, as one would indeed expect from homeostasis. We determine, in the stationary regime, the dependence of the mitochondrial variables on the respiration inputs, namely the cytosolic concentration of calcium Ca-c and the substrate fructose 1,6-bisphosphate FBP.

The same dynamical effects of calcium and FBP saturations reported for the original BPLS model are observed here. We find out, however, a novel nonstationary effect, which could be, in principle, physiologically interesting: some response times of the model tend to increase considerably for high concentrations of calcium and/or FBP. In particular, the larger the concentrations of Ca-c and/or FBP, the larger the necessary time to attain homeostasis.

Bulletin Of Mathematical Biology 75[9], 1636-1651, 2013. DOI: 10.1007/s11538-013-9862-1

[P266-2013] "Motional entanglement with trapped ions and a nanomechanical resonator"

Nicacio, F.*; Furuya, K.*; Semiao, F. L.

We study the entangling power of a nanoelectromechanical system (NEMS) simultaneously interacting with two separately trapped ions. To highlight this entangling capability, we consider a special regime where the ion-ion coupling does not generate entanglement in the system and any resulting entanglement will be the result of the NEMS acting as an entangling device. We study the dynamical behavior of the bipartite NEMS-induced ion-ion entanglement as well as the tripartite entanglement of the whole system (ions + NEMS). We found some quite remarkable phenomena in this hybrid system. For instance, the two trapped ions initially uncorrelated and prepared in coherent states can become entangled by interacting with a nanoelectromechanical resonator (also prepared in a coherent state) as soon as the ion-NEMS coupling achieves a certain value, and this can be controlled by external voltage gate on the NEMS device. We also show that, dynamically, the tripartite entanglement presents a more pronounced robustness against the destructive effects of dissipation when compared to the bipartite content.

Physical Review A 88[2], 022330, 2013. DOI: 10.1103/PhysRevA.88.022330

[P267-2013] "Nanometric particle size and phase controlled synthesis and characterization of gamma-Fe2O3 or (alpha plus gamma)-Fe2O3 by a modified sol-gel method"

Silva, M. F.; **de Oliveira, L. A. S.***; Ciciliati, M. A.; Silva, L. T.; Pereira, B. S.; Hechenleitner, A. A. W.; Oliveira, D. M. F.; **Pirota, K. R.***; Ivashita, F. F.; Paesano, A. Jr.; Pastor, J. M.; Perez-Landazabal, J. I.; Pineda, E. A. G.

Fe2O3 nanoparticles with sizes ranging from 15 to 53 nm were synthesized by a modified sol-gel method. Maghemite particles as well as particles with admixture of maghemite and hematite were obtained and characterized by XRD, FTIR, UV-Vis photoacoustic and Mossbauer spectroscopy, TEM, and magnetic measurements. The size and hematite/maghemite ratio of the nanoparticles were controlled by changing the Fe:PVA (poly (vinyl alcohol)) monomeric unit ratio used in the medium reaction (1:6, 1:12, 1:18, and 1:24). The average size of the nanoparticles decreases, and the maghemite content increases with increasing PVA amount until 1:18 ratio. The maghemite and hematite nanoparticles showed cubic and hexagonal morphology, respectively. Direct band gap energy were 1.77 and 1.91 eV for A6 and A18 samples. Zero-field-cooling-field-cooling curves show that samples present superparamagnetic behavior. Maghemite-hematite phase transition and hematite Neel transition were observed near 700K and 1015 K, respectively. Magnetization of the particles increases consistently with the increase in the amount of PVA used in the synthesis. Mossbauer spectra were adjusted with a hematite sextet and maghemite distribution for A6, A12, and A24 and with maghemite distribution for A18, in agreement with XRD results.

Journal Of Applied Physics 114[10], 104311, 2013. DOI: 10.1063/1.4821253

[P268-2013] "One Step Chemical Synthesis of Ag-Fe3O4 Heterodimer Nanoparticles: Optical, Structure, and Magnetic Properties"

Muraca, D.*; Odio, O. F.; Reguera, E.; **Pirota, K. R.***

Optical, magnetic and structural properties of one-step chemical decomposition approach Ag-Fe3O4 heterodimer structures are reported. We synthesized Ag-Fe3O4 nanoparticles where the Ag nanoparticles of less than 10 nm are physically attached to Fe3O4 nanoparticles also less than 10 nm. The structural properties of the samples were characterized from X-ray diffraction (XRD) and transmission electron microscopy (TEM) data, which confirmed the existence of heterodimer structures in solution along with isolated magnetite nanoparticles. Optical properties of the obtained samples were studied using UV/vis spectra and compared with Fe3O4 reference nanoparticles in absence of metallic component. Magnetization hysteresis loops for the obtained samples along with Fe3O4 reference sample at 2 K (blocked regime), 50 K (intermediate regime) and 300 K (superparamagnetic regime) and with maximum applied field of +/- 20 kOe were performed and correlated to the structural data. Also, magnetization versus temperature curves (Field Cooling-Zero Field Cooling) with static magnetic field of 50 Oe were measured, from which the blocking temperature of the heterodimer sample was about 77 K and for the reference less than 20 K.

IEEE Transactions On Magnetics 49[8], 4606-4609, Parte 1, 2013. DOI: 10.1109/TMAG.2013.2259148

[P269-2013] "Optical properties of charged quantum dots doped with a single magnetic impurity"

Mendes, U. C.*; Korkusinski, M.; Trojnar, A. H.; Hawrylak, P.

We present a microscopic theory of the optical properties of self-assembled quantum dots doped with a single magnetic manganese (Mn) impurity and containing a controlled number of electrons. The single-particle electron and heavy-hole electronic shells are described by two-dimensional harmonic oscillators. The electron-electron, electron-hole Coulomb as well as the short-range electron spin-Mn spin and hole spin-Mn spin contact exchange interactions are included. The electronic states of the photoexcited electron-hole-Mn complex and of the final electron-Mn complex are expanded in a finite number of configurations and the full interacting Hamiltonian is diagonalized numerically. The emission spectrum is predicted as a function of photon energy for a given number of electrons and different number of confined electronic quantum dot shells. We show how emission spectra allow to identify the number of electronic shells, the number of electrons populating these shells and, most importantly, their spin. We show that electrons not interacting directly with the spin of Mn ion do so via electron-electron interactions. This indirect interaction is a strong effect even when Mn impurity is away from the quantum dot center.

Physical Review B 88[11], 115306, 2013. DOI: 10.1103/PhysRevB.88.115306

[P270-2013] "Osteoblastic potency of bone marrow cells cultivated on functionalized biometals with cyclic RGD-peptide"

Jaeger, M.; Boege, C.; **Janissen, R.***; Rohrbeck, D.; Huelsen, T.; Lensing-Hoehn, S.; Krauspe, R.; Herten, M.

The fixation of cementless endoprostheses requires excellent fixation at the bone implant interface. Although the surface structures of these implants are designed to promote osteoblastic differentiation, poor bone quality may prevent or delay osseointegration. There is evidence that RGD peptides known as recognition motifs for various integrins, promote cellular adhesion, influence cellular proliferation, and differentiation of local cells. In this study, five different metal surfaces were analyzed: Sandblasted (TiSa) and polished (TiPol) Ti6Al4V, porocoated (CCPor) and polished (CCPol) cobalt chrome and polished stainless steel (SS) were coated by ethanol amine and poly(ethylene glycol) to attach covalently RGD peptides. Human mesenchymal stromal cells of healthy donors were cultivated onto prior functionalized metal surfaces for 14 days without osteogenic stimulation. Cell proliferation and differentiation were quantitatively evaluated for native (I), NaOH pre-activated (II), NaOH pre-activated, and PEG-coated (III) as well as for RGD (IV) coated surfaces. The RGD immobilization efficiency was analyzed by epi-fluorescence spectroscopy, cell morphology was documented by light and scanning electron microscopy. The RGD-binding efficiency was TiSa > TiPol > SS > CCPor > CCPol. RGD coated surfaces showed the highest average cell proliferation on CCPol > SS > CCPor > TiSa TiPol, whereas cellular differentiation mostly correlated with the observed proliferation results, such as CCPol > TiSa > SS > CCPor > TiPol. Considering statistical analyses (significance level of = 0.05), the RGD-coating of all biometals in comparison and in respect of their particular controls showed no significant improvement in cellular proliferation and osteoblastic differentiation.

Journal Of Biomedical Materials Research Part A 101[10], 2905-2914, 2013. DOI: 10.1002/jbm.a.34590

[P271-2013] “Photocatalytic hydrogen production of Co(OH)(2) nanoparticle-coated alpha-Fe2O3 nanorings”

Wender, H.; Goncalves, R. V.; **Dias, C. S. B.***; Zapata, M. J. M.; **Zagonel, L. F.***; Mendonca, E. C.; Teixeira, S. R.; Garcia, F.

The production of hydrogen from water using only a catalyst and solar energy is one of the most challenging and promising outlets for the generation of clean and renewable energy. Semiconductor photocatalysts for solar hydrogen production by water photolysis must employ stable, non-toxic, abundant and inexpensive visible-light absorbers capable of harvesting light photons with adequate potential to reduce water. Here, we show that alpha-Fe2O3 can meet these requirements by means of using hydrothermally prepared nanorings. These iron oxide nanoring photocatalysts proved capable of producing hydrogen efficiently without application of an external bias. In addition, Co(OH)(2) nanoparticles were shown to be efficient co-catalysts on the nanoring surface by improving the efficiency of hydrogen generation. Both nanoparticle-coated and uncoated nanorings displayed superior photocatalytic activity for hydrogen evolution when compared with TiO2 nanoparticles, showing themselves to be promising materials for water-splitting using only solar light.

Nanoscale 5[19], 9310-9316, 2013. DOI: 10.1039/c3nr02195e

[P272-2013] “Positron and electron collisions with nitrous oxide: Measured and calculated cross sections”

Chiari, L.; Zecca, A.; Trainotti, E.; Garcia, G.; Blanco, F.; Bettega, M. H. F.; Sanchez, S. D.; Varella, M. T. D.; **Lima, M. A. P.***; Brunger, M. J.

We present cross-section results from an experimental and theoretical study on positron scattering from nitrous oxide. Total cross sections (TCSs) have been measured at incident energies between 0.1 and 70 eV with a linear-transmission-based positron spectrometer. Elastic differential and integral cross sections, as well as inelastic integral cross sections and TCSs, have been computed with two different theoretical approaches: the independent atom model with screening-corrected additivity rule (IAM-SCAR), at energies in the 1- to 1000-eV range, and the Schwinger multichannel method at energies between 0.1 and 10 eV. Note that the latter method specifically reports cross sections for the elastic channel. We find good qualitative agreement between the theories and the TCS experiment at all common energies. That level of accord is found to also become quantitative above the ionization energy of nitrous oxide. Electron-impact TCSs calculated with the IAM-SCAR approach are also presented and compared to the existing results in order to uncover any similarities or differences in the scattering processes between these two leptons and nitrous oxide.

Physical Review A 88[2], 022708, 2013. DOI: 10.1103/PhysRevA.88.022708

[P273-2013] “Probing non-standard interaction of neutrinos with Ice Cube and Deep Core”

Esmaili, A.*; Smirnov, A. Y.

We consider effects of the Non-Standard Interactions (NSI) on oscillations of the high energy atmospheric neutrinos. The v(mu)-oscillograms are constructed and their dependence on the NSI strength parameters epsilon(alpha beta) studied. We computed the zenith angle distributions of the v(mu)-events in the presence of NSI in different energy regions. The distributions are confronted with the IceCube-79 (high energy sample) and the DeepCore (low energy sample) data and constraints on the strength parameters vertical bar epsilon(mu T)vertical bar less than or similar to 6 x 10(-3) and vertical bar epsilon mu mu - epsilon tau tau vertical bar x 10(-2) (90% C.L.) have been obtained. Future measurements of the zenith angle distributions by DeepCore in several energy bins will allow to improve the bounds by factor 2-3. We discuss the signatures of NSI in the zenith angle and energy distributions of events which allow to discriminate them from the effects of sterile neutrinos.

Journal Of High Energy Physics 6[026], 2013. DOI: 10.1007/JHEP06(2013)026

[P274-2013] “Role of instabilities in the survival of quantum correlations”

Roque, T. F.*; Roversi, J. A.*

This article surveys quantum correlations dynamics, in the Markovian and non-Markovian regimes, in a system of two harmonic oscillators connected by a time-dependent coupling and in contact with a common heat bath. The results show the survival of the quantum correlations, including entanglement, even at very high temperatures, as well as a remarkable relation between entanglement and the instability of the system. The results also show that the indirect interaction of the oscillators via a bath significantly enhances the quantum correlations and that quantum correlations are much more sensitive to the parameters of the oscillators than the temperature of the bath.

Physical Review A 88[3], 032114, 2013. DOI: 10.1103/PhysRevA.88.032114 Publicado: SEP 23 2013

[P275-2013] “Screening vector field modifications of general relativity”

Jimenez, J. B.; **Froes, A. L. D.*;** Mota, D. F.

A screening mechanism for conformal vector-tensor modifications of general relativity is proposed. The conformal factor depends on the norm of the vector field and makes the field to vanish in high dense regions, whereas drives it to a non-null value in low density environments. Such process occurs due to a spontaneous symmetry breaking mechanism and gives rise to both the screening of fifth forces as well as Lorentz violations.

The cosmology and local constraints are also computed.

Physics Letters B 725[4-5], 212-217, 2013. DOI: 10.1016/j.physletb.2013.07.032

[P276-2013] "Search for gluino mediated bottom- and top--squark production in multijet final states in pp collisions at 8 TeV"

Chatrchyan, S.; Khachatryan, V.; Sirunyan, A. M.; Tumasyan, A.; **Chinellato, J.*; Tonelli Manganote, E. J.*;** et al.
CMS Collaboration

A search for supersymmetry is presented based on events with large missing transverse energy, no isolated electron or muon, and at least three jets with one or more identified as a bottom-quark jet. A simultaneous examination is performed of the numbers of events in exclusive bins of the scalar sum of jet transverse momentum values, missing transverse energy, and bottom-quark jet multiplicity. The sample, corresponding to an integrated luminosity of 19.4 fb(-1), consists of proton--proton collision data recorded at a center-of-mass energy of 8 TeV with the CMS detector at the LHC in 2012. The observed numbers of events are found to be consistent with the standard model expectation, which is evaluated with control samples in data. The results are interpreted in the context of two simplified supersymmetric scenarios in which gluino pair production is followed by the decay of each gluino to an undetected lightest supersymmetric particle and either a bottom or top quark-antiquark pair, characteristic of gluino mediated bottom- or top-squark production. Using the production cross section calculated to next-to-leading-Order plus next-to-leading-logarithm accuracy, and in the limit of a massless lightest supersymmetric particle, we exclude gluinos with masses below 1170 GeV and 1020 GeV for the two scenarios, respectively.

Physics Letters B 725[4-5], 243-270, 2013. DOI: 10.1016/j.physletb.2013.06.058

[P277-2013] "Search for microscopic black holes in pp collisions at root s=8 TeV"

Chatrchyan, S.; Khachatryan, V.; Sirunyan, A. M.; Tumasyan, A.; Adam, W.; **Chinellato, J.*; Tonelli Manganote, E. J.*;** et al.
CMS Collaboration

A search for microscopic black holes and string balls is presented, based on a data sample of pp collisions at root s = 8 TeV recorded by the CMS experiment at the Large Hadron Collider and corresponding to an integrated luminosity of 12 fb(-1). No excess of events with energetic multiparticle final states, typical of black hole production or of similar new physics processes, is observed. Given the agreement of the observations with the expected standard model background, which is dominated by QCD multijet production, 95% confidence level limits are set on the production of semiclassical or quantum black holes, or of string balls, corresponding to the exclusions of masses below 4.3 to 6.2 TeV, depending on model assumptions. In addition, model-independent limits are set on new physics processes resulting in energetic multiparticle final states.

Journal Of High Energy Physics 7, UNSP 178, 2013. DOI: 10.1007/JHEP07(2013)178

[P278-2013] "Searches for long-lived charged particles in pp collisions at root s=7 and 8 TeV"

Chatrchyan, S.; Khachatryan, V.; Sirunyan, A. M.; Tumasyan, A.; Adam, W.; **Chinellato, J.*; Tonelli Manganote, E. J.*;** et al.
CMS Collaboration

Results of searches for heavy stable charged particles produced in pp collisions at root s = 7 and 8 TeV are presented corresponding to an integrated luminosity of 5.0 fb(-1) and 18.8 fb(-1), respectively. Data collected with the CMS detector are used to study the momentum, energy deposition, and time-of-flight of signal candidates. Leptons with an electric charge between e/3 and 8e, as well as bound states that can undergo charge exchange with the detector material, are studied. Analysis results are presented for various combinations of signatures in the inner tracker only, inner tracker and muon detector, and muon detector only. Detector signatures utilized are long time-of-flight to the outer muon system and anomalously high (or low) energy deposition in the inner tracker. The data are consistent with the expected background, and upper limits are set on the production cross section of long-lived gluinos, scalar top quarks, and scalar tau leptons, as well as pair produced long-lived leptons. Corresponding lower mass limits, ranging up to 1322 GeV/c(2) for gluinos, are the most stringent to date.

Journal Of High Energy Physics 7, 122, 2013. DOI: 10.1007/JHEP07(2013)122

[P279-2013] "Structural Distortion and Magnetic Order in the Intermetallic Eu3Ir4Sn13 Compound"

Mardegan, J. R. L.*; Aliouane, N.; Coelho, L. N.; **Aguero, O.*;** Bittar, E. M.; Lang, J. C.; **Pagliuso, P. G.*; Torriani, I. L.*; Giles, C.***

In this work, we have investigated the low temperature structural distortion and magnetic properties of the Eu3Ir4Sn13 Remeika cubic phase compound using X-ray powder diffraction (XRD), X-ray resonant magnetic scattering (XRMS) and neutron diffraction. X-ray scattering revealed that the peak observed in electrical resistivity and heat capacity measurements is related to a structural distortion at T* = 57.1 K. This crystallographic distortion characterized by the arising of a propagation vector (q) over right arrow = (0, (1/2), (1/2)) is due to a displacement of the Sn ions at the Sn1Sn2(12) polyhedron. In addition, the neutron diffraction experiments performed on a single crystal of Eu3Ir4Sn13 exhibit an antiferromagnetic coupling below T-N = 10.1 K where we observe a commensurate magnetic propagation vector (tau) over right arrow = (0, (1/2), (1/2)) identical to the one observed for the structural distortion.

IEEE Transactions On Magnetics 49[8], 4652-4655, Parte 1, 2013. DOI: 10.1109/TMAG.2013.2255589

[P280-2013] "Study of exclusive two-photon production of W+W- in pp collisions at root s=7 TeV and constraints on anomalous quartic gauge couplings"

Chatrchyan, S.; Khachatryan, V.; Sirunyan, A. M.; Tumasyan, A.; Adam, W.; **Chinellato, J.*; Tonelli Manganote, E. J.*;** et al.
CMS Collaboration

A search for exclusive or quasi-exclusive W+W- production by photon-photon interactions, pp -> p(*)W(+)W(-)p(*), at \/s = 7 TeV is reported using data collected by the CMS detector with an integrated luminosity of 5.05 fb(-1). Events are selected by requiring a mu(+/-)mu(-/+) vertex with no additional associated charged tracks and dilepton transverse momentum p(T)(mu(+/-)mu(-/+)) > 30 GeV. Two events passing all selection requirements are observed in the data, compared to a standard model expectation of 2.2 +/- 0.4 signal events with 0.84 +/- 0.15 background. The tail of the dilepton p(T) distribution is studied for deviations from the standard model. No events are observed with p(T) > 100 GeV. Model-independent upper limits are computed and compared to predictions involving anomalous quartic gauge couplings.

The limits on the parameters a(0,c)(W)/A(2) with a dipole form factor and an energy cutoff A(cutoff) = 500 GeV are of the order of 10(-4).

Journal Of High Energy Physics 7, 116, 2013. DOI: 10.1007/JHEP07(2013)116

[P281-2013] "Study of the underlying event at forward rapidity in pp collisions at root s=0.9, 2.76, and 7 TeV"

Chatrchyan, S.; Khachatryan, V.; Sirunyan, A. M.; Tumasyan, A.; Adam, W.; **Chinellato, J.*; Tonelli Manganote, E. J.***; et al.
CMS Collaboration

The underlying event activity in proton-proton collisions at forward pseudorapidity (-6.6 < eta < -5.2) is studied with the CMS detector at the LHC, using a novel observable: the ratio of the forward energy density, dE/d(eta), for events with a charged-particle jet produced at central pseudorapidity (vertical bar eta(jet)vertical bar < 2) to the forward energy density for inclusive events. This forward energy density ratio is measured as a function of the central jet transverse momentum, p(T), at three different pp centre-of-mass energies (root s = 0.9, 2.76, and 7 TeV). In addition, the root s evolution of the forward energy density is studied in inclusive events and in events with a central jet. The results are compared to those of Monte Carlo event generators for pp collisions and are discussed in terms of the underlying event. Whereas the dependence of the forward energy density ratio on jet p(T), at each root s separately can be well reproduced by some models, all models fail to simultaneously describe the increase of the forward energy density with root s in both inclusive events and in events with a central jet.

Journal Of High Energy Physics 4, 072, 2013. DOI: 10.1007/JHEP04(2013)072

[P282-2013] "Synthesis and Characterization of Iron Oxyhydroxide Nanowires"

Londono-Calderon, C. L.; Bilovol, V.; Cosio-Castaneda, C.; Pampillo, L. G.; Micheli, S. R.; **Pirota, K. R.***; Socolovsky, L. M.; Martinez-Garcia, R.

A very simple method of synthesis of goethite, alpha - FeOOH, nanowire is reported. To fabricate the nanowires, an anodized alumina nanoporous template (AAO) is used. AAO has pores with an average diameter of 60 nm. The synthesis is based on a self-combustion reaction of the chemical precursor (Fe(NO3)(3) saturated solution) which occurs inside the nanopores. The geometry of AAO determines the morphology of the nanowires and the confinement conditions in which the heat treatment determines the composition of the nanostructure. The nanowires are characterized using scanning electron microscopy, high resolution transmission electron microscopy and magnetometry [magnetization versus applied field (M versus H)]. TEM analysis indicates that nanowires are composed of several alpha - FeOOH single crystals. The nanowires have a clear magnetic oriented structure.

IEEE Transactions On Magnetics 49[8], 4502-4505, Parte 1, 2013. DOI: 10.1109/TMAG.2013.2255027

[P283-2013] "Thalamic metabolic abnormalities in patients with Huntington's disease measured by magnetic resonance spectroscopy"

Casseb, R. F.*; D'Abreu, A.; Ruocco, H. H.; Lopes-Cendes, I.; Cendes, F.; **Castellano, G.***

Huntington's disease (HD) is a neurologic disorder that is not completely understood; its fundamental physiological mechanisms and chemical effects remain somewhat unclear. Among these uncertainties, we can highlight information about the concentrations of brain metabolites, which have been widely discussed. Concentration differences in affected, compared to healthy, individuals could lead to the development of useful tools for evaluating the progression of disease, or to the advance of investigations of different/alternative treatments. The aim of this study was to compare the thalamic concentration of metabolites in HD patients and healthy individuals using magnetic resonance spectroscopy. We used a 2.0-Tesla magnetic field, repetition time of 1500 ms, and echo time of 135 ms. Spectra from 40 adult HD patients and 26 control subjects were compared. Quantitative analysis was performed using the LCModel method. There were statistically significant differences between HD patients and controls in the concentrations of N-acetylaspartate + N-acetylaspartylglutamate (NAA + NAAG; t-test, P<0.001), and glycerophosphocholine + phosphocholine (GPC + PCh; t-test, P = 0.001) relative to creatine + phosphocreatine (Cr + PCr). The NAA + NAAG/Cr + PCr ratio was decreased by 9% and GPC + PCh/Cr + PCr increased by 17% in patients compared with controls. There were no correlations between the concentration ratios and clinical features. Although these results could be caused by T1 and T2 changes, rather than variations in metabolite concentrations given the short repetition time and long echo time values used, our findings point to thalamic dysfunction, corroborating prior evidence.

Brazilian Journal Of Medical And Biological Research 46[8], 722-727, 2013. DOI: 10.1590/1414-431X20132332

[P284-2013] "The Effect of Coated-Fe3O4 Nanoparticles on Magnetic Properties of Ferrogels Produced by Diffusion Route"

Moscoso-Londono, O.; **Muraca, D.*; de Oliveira, L. A. S.*; Pirota, K. R.***; Socolovsky, L. M.

In this paper, we report a novel, nontoxic and environmentally friendly diffusion route to obtain superparamagnetic poly(vinyl alcohol) (PVA)/polyacrylic acid (PAA) coated-Fe3O4 ferrogels (D-PAA). Magnetic properties of these D-PAA ferrogels were compared with regular ones produced with noncoated magnetite nanoparticles (D-NC). Their morphological features were studied by SEM-FEG. Absorption tests were performed in order to assess diffusion of nanoparticles into the PVA-polymeric matrix. D-PAA samples exhibit better dispersion of the nanoparticles within polymeric matrix in comparison with D-NC samples. The effective diffusion coefficients (D-eff) obtained, as well as the nature of the functional groups in question, suggests interactions between the PAA and PVA in D-PAA samples. In D-NC samples is presumed that the iron atoms in the surface of the nanoparticles act as Lewis acids and coordinates with molecules that donate lone-pair electrons. The results suggest a reduction in the magnetic interaction for the coated nanoparticles case, due to the improvement of the dispersion of the nanoparticles into the polymeric matrix.

IEEE Transactions On Magnetics 49[8], 4551-4554, Parte 1, 2013. DOI: 10.1109/TMAG.2013.2259804

[P285-2013] "The Severity of Osteogenesis Imperfecta and Type I Collagen Pattern in Human Skin as Determined by Nonlinear Microscopy: Proof of Principle of a Diagnostic Method"

Adur, J.*; DSouza-Li, L.; Pedroni, M. V.; Steiner, C. E.; Pelegati, V. B.; **de Thomaz, A. A.***; Carvalho, H. F.; **Cesar, C. L.***

Background: The confirmatory diagnosis of Osteogenesis Imperfecta (OI) requires invasive, commonly bone biopsy, time consuming and destructive methods. This paper proposes an alternative method using a combination of two-photon excitation fluorescence (TPEF) and second-harmonic generation (SHG) microscopies from easily obtained human skin biopsies.

We show that this method can distinguish subtypes of human OI. Methodology/Principal Findings: Different aspects of collagen microstructure of skin fresh biopsies and standard H&E-stained sections of normal and OI patients (mild and severe forms) were distinguished by TPEF and SHG images. Moreover, important differences between subtypes of OI were identified using different methods of quantification such as collagen density, ratio between collagen and elastic tissue, and gray-level co-occurrence matrix (GLCM) image-pattern analysis. Collagen density was lower in OI dermis, while the HG/autofluorescence index of the dermis was significantly higher in OI as compared to that of the normal skin. We also showed that the energy value of GLCM texture analysis is useful to discriminate mild from severe OI and from normal skin. Conclusions/Significance: This work demonstrated that nonlinear microscopy techniques in combination with image-analysis approaches represent a powerful tool to investigate the collagen organization in skin dermis in patients with OI and has the potential to distinguish the different types of OI. The procedure outlined in this paper requires a skin biopsy, which is almost painless as compared to the bone biopsy commonly used in conventional methods. The data presented here complement existing clinical diagnostic techniques and can be used as a diagnostic procedure to confirm the disease, evaluate its severity and treatment efficacy.

Plos One 8[7], e69186, 2013. DOI: 10.1371/journal.pone.0069186

[P286-2013] "The waveform digitiser of the Double Chooz experiment: performance and quantisation effects on photomultiplier tube signals"

Abe, Y.; Akiri, T.; Cabrera, A.; Courty, B.; Dawson, J. V.; **Gonzalez, L. F. G.*;** Hourlier, A.; Ishitsuka, M.; de Kerret, H.; Kryn, D.; Novella, P.; Obolensky, M.; Perasso, S.; Remoto, A.; Roncin, R.

We present the waveform digitiser used in the Double Chooz experiment. We describe the hardware and the custom-built firmware specifically developed for the experiment. The performance of the device is tested with regards to digitising low light level signals from photomultiplier tubes and measuring pulse charge. This highlights the role of quantisation effects and leads to some general recommendations on the design and use of waveform digitisers.

Journal Of Instrumentation 8, P08015, 2013. DOI: 10.1088/1748-0221/8/08/P08015

[P287-2013] "Tuning the giant inverse magnetocaloric effect in Mn2-xCrxSb compounds"

Caron, L.*; Miao, X. F.; Klaasse, J. C. P.; **Gama, S.*;** Bruck, E.

Structural, magnetic, and magnetocaloric properties of Mn2-xCrxSb compounds have been studied. In these compounds, a first order magnetic phase transition from the ferrimagnetic to the antiferromagnetic state occurs with decreasing temperature, giving rise to giant inverse magnetocaloric effects that can be tuned over a wide temperature interval through changes in substitution concentration. Entropy changes as high as 7.5 J/kgK have been observed, and a composition independent entropy change is obtained for several different concentrations/working temperatures, making these compounds suitable candidates for a composite working material.

Applied Physics Letters 103[11], 112404, 2013. DOI: 10.1063/1.4821197

[P288-2013] "Water Exclusion Layers Probed by Depth Scan Confocal Raman Microscopy"

Teschke, O.*; Bonugli, L. O.*; dos Santos, M. V. P.*

Depth scan confocal Raman microscopy was employed to map water and air spatial distributions in immersed superhydrophobic films. Due to the lack of visible nanobubbles on flat surfaces, we have probed heterogeneous surfaces where solid-liquid, liquid-vapor, and vapor-solid coexist. Depth scan profiles show liquid exclusion (vapor) layers inside the fiber arrangement and water in contact only at the fiber apex.

Microscopy And Microanalysis 19[5], 1317-1322, 2013. DOI: 10.1017/S1431927613001827

[P289-2013] "Widespread neuronal damage and cognitive dysfunction in spinocerebellar ataxia type 3"

Lopes, T. M.; D'Abreu, A.; Franca, M. C.; Yasuda, C. L.; Betting, L. E.; Samara, A. B.; **Castellano, G.*; Somazz, J. C.***; Balthazar, M. L. F.; Lopes-Cendes, I.; Cendes, F.

Previous studies demonstrated cognitive impairments in spinocerebellar ataxia type 3 (SCA3/MJD); however, there is no consensus about the cognitive domains affected and the correlation with structural brain abnormalities. We investigated the neuropsychological profile and 3T-MRI findings, including high-resolution T1-images, diffusion tensor imaging and magnetic resonance spectroscopy of 32 patients with SCA3/MJD and 32 age-, gender- and educational level-matched healthy controls. We reviewed patients' clinical history and CAG repeat length, and performed assessment and rating of ataxia (SARA)-Brazilian version and the neuropsychiatric inventory. Patients presented worse performance in episodic and working memory and Beck inventories (depression and anxiety). SCA3/MJD patients had a reduction of gray matter volume (GM) in the cerebellum, putamen, cingulum, precentral and parietal lobe. A positive correlation was identified between the cognitive findings and GM of temporal, frontal, parietal, culmen and insula. We observed positive correlation between the brainstem's fractional anisotropy and digit span-forward. The following cerebellar metabolite groups (measured relative to creatine) were reduced in patients: N-acetyl-aspartate (NAA), NAA + N-acetyl-aspartate-glutamate and glutamate + glutamine (Glx). We found a positive correlation between Corsi's block-tapping task forward with Glx; semantic verbal fluency with phosphorylcholine and glycerophosphorylcholine; digits span-forward with NAA. The cognitive impairments in SCA3/MJD are associated not only with cerebellar and brainstem abnormalities, but also with neuroimaging evidence of diffuse neuronal and axonal dysfunction, particularly in temporal, frontal, parietal and insular areas.

Journal Of Neurology 260[9], 2370-2379, 2013. DOI: 10.1007/s00415-013-6998-8

Proceedings

[P290-2013] “Multiphoton intravital microscopy setup to visualize the mouse mammary gland”

Adur, J.*; Torres, A. M. H.; Masedunskas, A.; Baratti, M. O.; **de Thomaz, A. A.***; Pelegati, V. B.; Carvalho, H. F.; **Cesar, C. L.*;** Beaurepaire E. (Ed.); So, P. T. C.(Ed.)

Recently, light microscopy-based techniques have been extended to live mammalian models leading to the development of a new imaging approach called intravital microscopy (IVM). Although IVM has been introduced at the beginning of the last century, its major advancements have occurred in the last twenty years with the development of non-linear microscopy that has enabled performing deep tissue imaging. IVM has been utilized to address many biological questions in basic research and is now a fundamental tool that provide information on tissues such as morphology, cellular architecture, and metabolic status. IVM has become an indispensable tool in numerous areas. This study presents and describes the practical aspects of IVM necessary to visualize epithelial cells of live mouse mammary gland with multiphoton techniques.

Advanced Microscopy Techniques III, Proceedings of SPIE 8797, UNSP 879705, 2013. DOI: 10.1117/12.2032439

Conference on Advanced Microscopy Techniques III, MAY 15-16, 2013, Munich, GERMANY.

*** Autores do Instituto de Física “Gleb Wataghin” - IFGW**

Defesas de Dissertações - Mestrado

[D018-13] “Estudo da difusão e tunelamento planares para a equação de Dirac em presença de potenciais eletrostáticos”
Aluno: Gabriel Gulak Maia
Orientador: Prof. Dr. Stefano De Leo
Data: 16/09/2013

[D019-13] “Propriedades estruturais e magnéticas de nanofios de cobalto eletrodepositados”
Aluno: Peterson Grandini de Carvalho
Orientador: Prof. Dr. Kleber Roberto Pirota
Data: 27/09/2013

[D020-13] “Estudo do tunelamento da magnetização em magnetos moleculares de Mn12 via q- histerons”
Aluno: Priscila Todero de Almeida
Orientador: Não informado
Data: 01/11/2013

Defesas de Teses - Doutorado

[T011-13] “Estudo de nanoestruturas de carbono em múltiplas escalas”
Aluno: Leonardo Dantas Machado
Orientador: Prof. Dr. Douglas Soares Galvão
Data: 24/09/2013

[T012-13] “Dinâmica molecular e peridynamics aplicadas a nanotecnologia. Um estudo sobre filmes finos e nanofios metálicos.”
Aluno: Zenner Silva Pereira
Orientador: Prof. Dr. Edison Zacarias da Silva
Data: 11/10/2013

[T013-13] “Estudos do modelo de Hubbard desordenado em duas dimensões”
Aluno: Martha Yolima Suárez Villagrán
Orientador: Prof. Dr. Eduardo Miranda
Data: 18/10/2013

[T014-13] “Estudo dos efeitos de flutuações da condição inicial em colisões nucleares relativísticas”
Aluno: Rafael Derradi de Souza
Orientador: Prof. Dr. Jun Takahashi
Data: 24/10/2013

[T015-13] “Pontos quânticos colidais de semicondutores: Sínteses, caracterizações e aplicações”
Aluno: Diogo Burigo Almeida
Orientador: Prof. Dr. Carlos Lenz Cesar
Data: 25/10/2013

Fonte: Portal IFGW/PPós-graduação.
Disponível em: http://portal.ifi.unicamp.br/eventos#date=2013-05-01,mode=month

* Informamos que a partir de janeiro de 2014 o Boletim Abstracta será publicado somente em versão eletrônica! Continue recebendo seu boletim! Acesse o portal Abstracta e faça seu cadastro como leitor:

<http://abstracta.ifi.unicamp.br>

Abstracta

Instituto de Física
Diretor: Prof. Dr. Daniel Pereira
Diretor Associado: Prof. Dr. Newton Cesario Frateschi
Universidade Estadual de Campinas - UNICAMP
Cidade Universitária Zeferino Vaz
13083-859 - Campinas - SP - Brasil
e-mail: secdir@ifi.unicamp.br
Fone: 0XX 19 3521-5300

Publicação

Biblioteca do Instituto de Física Gleb Wataghin
http://portal.ifi.unicamp.br/biblioteca

Diretora Técnica: Sandra Maria Carlos Cartaxo
Coordenador da Comissão de Biblioteca: Prof. Dr. André Koch Torres de Assis

Elaboração
Maria Graciele Trevisan (Bibliotecária)
graciele@ifi.unicamp.br

Projeto Gráfico
ÍgneaDesign

Impressão: Gráfica Central - Unicamp